Preliminary Analyses of Apollo 15 Sample 15085 via X-Ray Computed Tomography. A. J. Gawronska[1], C. L. McLeod[1], E. H. Blumenfeld[2], R. Hanna[3], R. A. Zeigler[4]. [1]Dept. Of Geology & Envt. Earth Science, Miami University, Oxford OH, 45056. (gawronaj@miamioh.edu). [2]LZ Technology, JETS Contract, NASA Johnson Space Center, Houston TX, 77058, [3]Jackson School of Geosciences, University of Texas at Austin, Austin TX, 78712. [4]NASA Johnson Space Center, Houston TX, 77058.

Introduction: The broad aim of this research is to advance our understanding of the petrochemical and petrophysical characteristics of lunar basalts. This will be achieved through novel application of three dimensional X-ray computed tomography (XCT) scanning to the Apollo sample suite in order to discern what 3D information can be extracted from these samples to investigate the processes associated with the assembly of lunar magmas and their emplacement on the Moon.

Data acquired via XCT can be utilized to 1) evaluate the potential to characterize the flow fabrics and internal structure and patterns in the rock from preferential vesicle and/or mineral orientations [1], 2) determine mineral content based on volumetric calculations [2], and 3) attempt to establish particle size distributions using acquired 3D data as opposed to relying on calculations that may not account for mineral crystal habit heterogeneity [3, 4]. The data presented here is a preliminary look at how this 3D approach could begin to address the above research objectives.

This study follows the methods outlined in a number of meteoritical studies [1], and takes advantage of the 3D Virtual Astromaterials Samples Collection project at the NASA JSC Astromaterials Research and Exploration Science Division, currently under development by [5].

Methods: Sample 15085,0, an Apollo 15 pigeonite basalt [6], was scanned at the UTCT facility for NASA [5]. Complete documentation of the analytical methodology may be found in [1, 5, 7]. Once computed, scans were transformed using Dragonfly software [8] to exclude the outside of the sample by applying a grayscale value that may be easily excluded – the software automatically identifies all voxels that connect to background even indirectly through adjacent slices (**Fig. 1**). Scans were subsequently processed through Blob3D software [7] by separating scanned data into components based on grayscale differences, and segmenting these into individual "blobs" which represent the three-dimensional visualization of an object as defined by the grayscale (**Fig. 2)**. The data associated with volume and the axes of all "blobs" could then be exported to Excel for further analyses (**Table 1**). This exported dataset was reorganized and fed into Stereo32 software in order to determine if any orientation exists within similar componets (i.e. minerals) (**Fig. 3**).

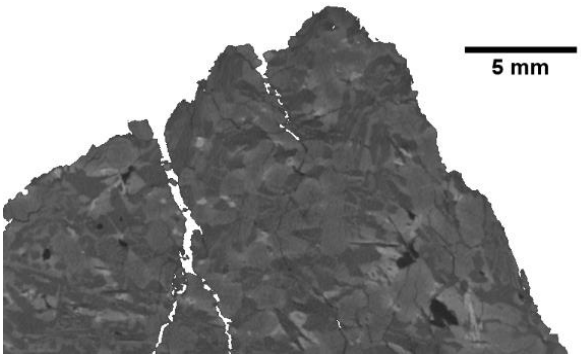

Figure 1. Image of a slice of sample 15085,0 – background has been fixed to a value of 255, or white, for easy omission. This image additionally highlights cracks that connect to outside and have been fixed.

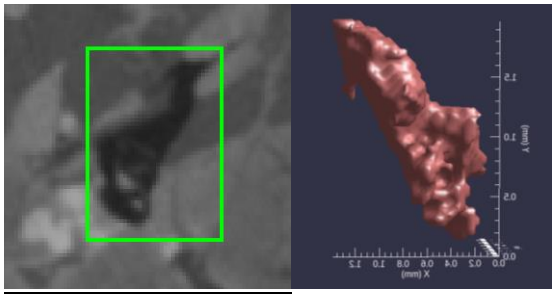

Figure 2. An area is signified by Blob3D (left) to contain a specific grayscale that represents a given component, in this case a vesicle containing growing or broken off grains within its interior. The signified area is then recreated by Blob3D into the specified blob (right). Axes shown for reference. The surface of the blob appears rugged due to the grains inside the vesicle that were not incorporated into the blob.

Results: Blob3D is successful at automatically separating phases based on grayscale values and extracting the volumes of individual components. In 15085,0, clinopyroxene (pigeonite) dominates the sample volumetrically as expected at approx. 65% volume. It is followed by plagioclase feldspar at approx. 21%, and opaques at ~1.5%, or up to ~3.5% if the harder-to-separate component titled "ungrouped light" is included (**Table 1**). These data match modal mineralogy observed in thin section by [10]. As indicated by the low volume of ungrouped leftovers, most voxels were successfully incorporated in a component.

Component Group	Grayscale	Vol. (mm^3)	% of total
Opaques	125-254	1135.08	1.57
Ungrouped Light	110-254	1423.06	1.97
Pyroxene	83-110	47089.31	65.24
Plagioclase	66-82	15279.21	21.17
Ungrouped Dark	40-70	6805.19	9.43
Vesicles	0-50	193.29	0.27
Ungrouped Left-overs	0-254	257.19	0.36
total	0-254	72182.32	100.00

Table 1. Summary of grayscale values used to separate voxels into phases and the corresponding volumes.

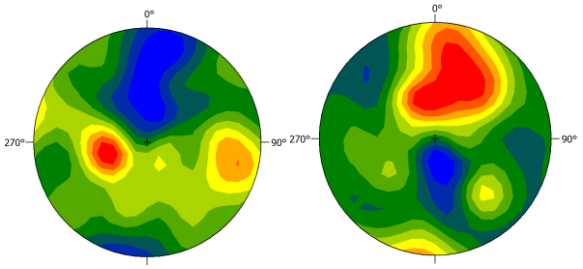

Figure 3. a) Stereonets for the long axis (left) and short axis (right) of vesicles (N=1780). The long axis exhibits a weak (C=0.135) girdle distribution (K=0.069); the short axis exhibits a weak (C=0.163) cluster distribution (K=3.693). Warm colors represent high number of objects oriented in the given direction.

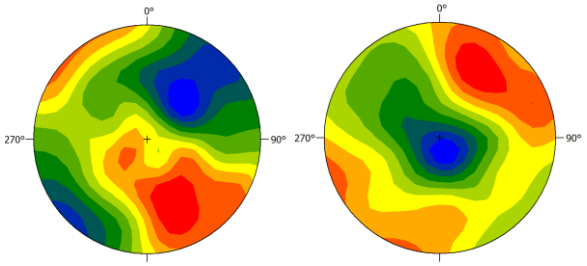

Figure 3. b) Stereonets for the long axis (left) and short axis (right) of opaque phases (N=14974). Both exhibit weak (C=0.092, C=0.135, respectively) girdle distributions (K=0.668, K=0.915, respectively).

Plagioclase and pyroxene crystals were highly interconnected and it was not possible to extract individual crystal data. The orientation of individual vesicles and opaque crystals, however, was successfully gathered (**Fig. 3**) – their relatively random distribution of orientations, as indicated by low C values [11], indicates that this particular lunar magma was potentially emplaced under low stress conditions.

Discussion: Due to the high linear attenuation of heavier atoms (i.e. Fe) opaque phases appear bright in the scans and are easier to separate [1, 2]. Phases such as pyroxene which can exhibit a wide range of compositions within a single crystal (i.e. due to zoning) produce grayscale values which are challenging to separate – hence the classification of an "ungrouped light" group on the threshold of values between particular pyroxene and opaque components. Upon closer inspection, this group is made up of both opaque phases and high-Fe pyroxene rims – manual segmentation may be necessary to group phases in such cases. Phases with narrow and similar grayscale value ranges are likewise difficult to separate – hence the existence of a leftover "ungrouped dark" group, which upon closer inspection is composed of tridymite laths, vesicles too small to contain a dark enough value to be incorporated into the vesicle component group, and cracks which add nonexistent volume. Segmenting only a part of the scanned sample (i.e. by using 20% of the collected slices) manually may fix this issue by adding human oversight and decreasing the amount of time necessary to complete the process. Overall, XCT is a powerful computational technique which may be used to preserve samples and utilized to evaluate the volume, foliation, and distribution of components within a rock. By visualizing these components in 3D, it should be further possible to distinguish individual minerals based on crystal habit.

This study will continue to evaluate the potential of XCT in providing data on the petrophysical characteristics of the Apollo lunar basalt suite using more samples. We intend to use this data to create 3D particle size distributions [2] and compare them to crystal size distributions calculated from 2D data [3, 4]. We will then analyze the major, minor, and trace element content of minerals in associated thin sections in order to enhance the characterization of physical and chemical attributes in the crystal cargoes of lunar basalts.

References: [1] Hanna R. D. & Ketcham R. A. (2017) *Chem. Erde 77*, 547-572. [2] Friedrich J. M. et al. (2008) *Planet. Space Sci. 56*, 895-900. [3] Morgan D. J. & Jerram D. A. (2006) *J. Volcanol. Geoth. Res. 154*, 1-7. [4] Higgins M. D. (2000) *Am. Mineral. 85*, 1105-1116. [5] Blumenfeld E. H. et al. (2017) *LPS XLXIII*, Abstract #2874. [6] Meyer C. (2010) Lunar Sample Compendium 15085. [7] Ketcham R. A. (2005) *Geosphere 1*, 32-41. [8] Object Research Systems Inc. (2016) www.theobjects.com/dragonfly. [9] Roller K. & Treppman C. (2007) www.ruhr-uni-bochum.de/hardrock/downloads.htm. [10] Brown G. M. et al. (1972) *PLSC 3*, 141-157. [11] Woodcock N. H. & Naylor M. A. (1983) *J. Struct. Geol. 5*, 539-548.

Acknowledgements: *These XCT image data were produced at the High-Resolution X-ray Computed Tomography Facility of the University of Texas at Austin for NASA's Acquisition & Curation Office and were funded by NASA Planetary Data Archiving, Restoration, and Tools Program, Proposal No.: 15-PDART15_2-0041.*